Research Article

Numerical evaluation of reinforced concrete slabs with fixed support under impact load

Tolga Yılmaz [a],* 🆔, Hasan Selim Şengel [b] 🆔

[a] *Department of Civil Engineering, Konya Technical University, 42250 Konya, Turkey*
[b] *Department of Civil Engineering, Eskişehir Osmangazi University, 26040 Eskişehir, Turkey*

ABSTRACT

Reinforced concrete (RC) structural members may be subjected to impact load besides quasi-static load or other dynamic loads like earthquake and wind loads in their service periods. Many research emphasized that although impact load acts on structural members for a short time, it caused considerable damage to these members or even collapses the whole structure. Thus, it becomes crucial to consider and accurately evaluate the impact load effect in the design process. The present study intends to introduce a finite element model (FEM) verified with the test data for the accurate evaluation of load-deflection behavior and damage patterns of the fixed supported RC slabs exposed to impact load. First, a nonlinear FEM including strain-rate effect for both concrete and steel reinforcement, and crack visualization algorithm has been established by using LS-DYNA software. Then, the dynamic responses obtained by the present FEM have been compared with the experimental data presented in a previous study existing in the literature and it is found that the present FEM yields accurate results for the RC slab subjected to impact load and it can be safely used in the design process. In the second part of the study, using the verified FEM, the effects of applied input impact energy, the application point of impact load, and hammer geometry on the dynamic responses and failure characteristics of the RC slabs exposed to the impact loading were investigated and interpreted in detail.

1. Introduction

Reinforced concrete (RC) slabs constitute functional areas in the structures. Besides, the main two duties of the RC slabs in the structural system are the transfer of the vertical loads to the beams, columns, load-bearing walls, and shear walls and the distribution of the lateral dynamic loads to vertical load-bearing structural members. The conventional design of the RC slab is performed by considering vertical loads such as dead and live loads and lateral earthquake and wind loads. However, recently, there is increasing concern about the design of the structural members against the low-velocity impact loads because there are many collision scenarios where velocities are up to 10 m/s in civil engineering. The rock fall, the vehicle crashes on bridge abutments,

aircraft landing on the airport runway, ice or ship collisions to offshore structures, and collisions of the masses drifted by the tsunami, flood, and landslide to the structures can be examples of impact scenarios (Yilmaz et al. 2022). Unlike static loads, impact loads generate the inertia effects and the strain-rate effects. Furthermore, although the impact loads act on structural elements in a very short time, they may lead to remarkable damage to structural members or even an entire collapse of the structure. Fig. 1 depicts some examples of the failure of the structural element and the collapse of the structures due to impact load. The disregarding impact load effect at the design level may cause damage or collapse. Therefore, the dynamic responses and failure characteristics of the RC structural members subjected to impact load should be determined and considered in the design

stage. However, the design concept for the RC elements against the impact loads has not been fully manifested, and also design codes do not recommend an obvious evaluation to calculate dynamic responses and determine impact-induced failure modes of RC members. Besides, since there is no fully accepted standard test setup in the literature for performing impact experiments, the researchers developed various test setups such as pendulum and drop weight to examine impact behavior (Sha and Hao 2013; Shi et al. 2021; Yilmaz et al. 2019). In the literature, there are many studies focused on parameters that can be effective on the impact response of the RC slabs. In these studies, the parameters such as the concrete compressive strength (Anas et al 2022a; Said and Mouwainea 2022), the steel reinforcement ratio (Mizushima et al. 2022; Yılmaz et al. 2020), the steel reinforcement placement inclinations (Vijay et al. 2020), the corroded steel rebars (Daneshvar et al. 2021), the thickness of the slab (Hering et al. 2020), the pre-stress and post-tensioned applica-

tions (Al Rawi et al. 2020; Kumar et al. 2018; Thai and Kim 2017), the support layouts (Anil et al. 2015; Yılmaz et al. 2020), the opening existing in the slab (Yilmaz et al. 2022) were studied. There are also studies related to the behavior of the RC slab strengthened with Carbon, Glass, and Bazalt Fiber Reinforced Polymer (FRP) subjected to impact load in the literature (Anas et al. 2022b; Almusallam et al. 2015; Chen et al. 2020; Radnić et al. 2015; Soltani et al. 2020; Yılmaz et al. 2018). Furthermore, the effect of the FRP rebars on impact responses of the slabs was also studied (Mousavi and Shafei 2019; Sadraie et al. 2019). Based on the experimental research investigated in the scope of the literature review performed, it can be concluded that impact experiments require specific test setups and advanced measurement techniques. At this point, for realistic and rapid evaluation of the impact resistance of the RC structural elements, it is worthwhile to say that the numerical studies based on the finite element method (FEM) have an important role.

Fig. 1. Collapse of structure/structural member due to impact load (Do et al. 2018).

Consequently, the main motivation of this study is to establish a FEM verified with test data to predict the dynamic response and damage characteristics of the RC slabs with fixed support. First, the FEM of the RC slabs, which considers the strain-rate effect for the concrete and steel materials and the crack visualization algorithm, by using LS-DYNA software has been introduced. The presented model is calibrated with the results obtained from an experimental study presented by Kumar et al. (2018). After the good agreement between test and numerical results was demonstrated, using the present model, a parametric study was carried out. In the parametric study, the effects of applied input impact energy, the application point of impact load, and hammer geometry on the impact behavior of the RC slabs are investigated and interpreted in detail.

2. Details of the Experiment used for Verification of Numerical Analysis

The comprehensive experimental study presented by Kumar et al. (2018) in which the conventional reinforced concrete (RC) and prestressed concrete plates subjected to impact force is investigated has been utilized for veri-

fication of the presented numerical model. In the experimental program, two RC slabs with dimensions of 800x800x100 mm. The concrete compressive strength after 28 days from the cast was determined as 48.4 MPa. The maximum size of coarse aggregate used for the manufacture of the RC slabs was 10 mm. Besides, natural sand was used as fine aggregate. The Ordinary Portland Cement of 43 grade has been used for the concrete mix. The ratio of concrete mix ingredients was 1:1.74:1.68 (cement/fine aggregate/coarse aggregate). The RC slab was designed using deformed steel rebars with high yield strength. The diameter of the steel bars was 8 mm. The steel rebars were spaced at 140 mm in the two directions of the RC slab. The average yield strength of the rebars was determined as 609 MPa with a uniaxial tension test. In the experimental program conducted by Kumar et al (2018), the RC slabs tested under impact load had fixed boundary conditions. The rotations and translations of plate edges were constrained. Impact energy has been applied to the center of the RC slabs by dropping freely a steel hammer. The weight of the hammer was 242.85 kg. The geometric shape of the hammer was a cylinder with a diameter of 100 mm. The input impact energies transferred to two RC slabs are 1.190 kJ and 2.380 kJ, which corresponds hammer drop heights of

500 mm and 1000 mm, respectively. The dimensions and rebar arrangement of the RC slabs and the setup used for carrying out experiments are illustrated in Fig. 2(a) and Fig. 2(b), respectively. The time histories of the impact load acting on the RC slabs and the displacements measured from the center point of the RC slabs on the tension side, recorded during tests, have been used to verify the presented FEM of the RC slabs. Furthermore, impact load-induced crack on the tension side of the two RC slabs has been compared to damage distributions obtained by the numerical model.

3. Details of the Presented FEM Model

In the study, LS-DYNA software is utilized for the generation of the FEM of the RC slabs with fixed support under the impact load. (LS-DYNA Keyword user's manual 2018). LS-DYNA could conduct nonlinear dynamic analysis using an explicit solver. Furthermore, LS-DYNA includes several concrete material models such as Winfrith Model, Continuous Surface Cap Model, and Concrete Damage Model (MAT_072R3) to model concrete material exposed to impulsive loading. Thus, LS-DYNA software is commonly preferred by structural engineers to evaluate the dynamic responses and failure characteristics of structural members exposed to blast and impact loads (Li et al. 2017; Chen et al. 2015, 2020; Do et al. 2018a, 2018b). The presented FEM is composed of four main parts: the RC slab, steel reinforcement, the rigid hammer, and rigid support. An 8-node hexahedron solid element with tri-linear shape functions, using one-point integration plus viscous hourglass control is used for modeling the concrete slab, hammer, and support while steel rebars were modeled by Hughes-Liu beam element with 2×2 Gauss quadrature integration.
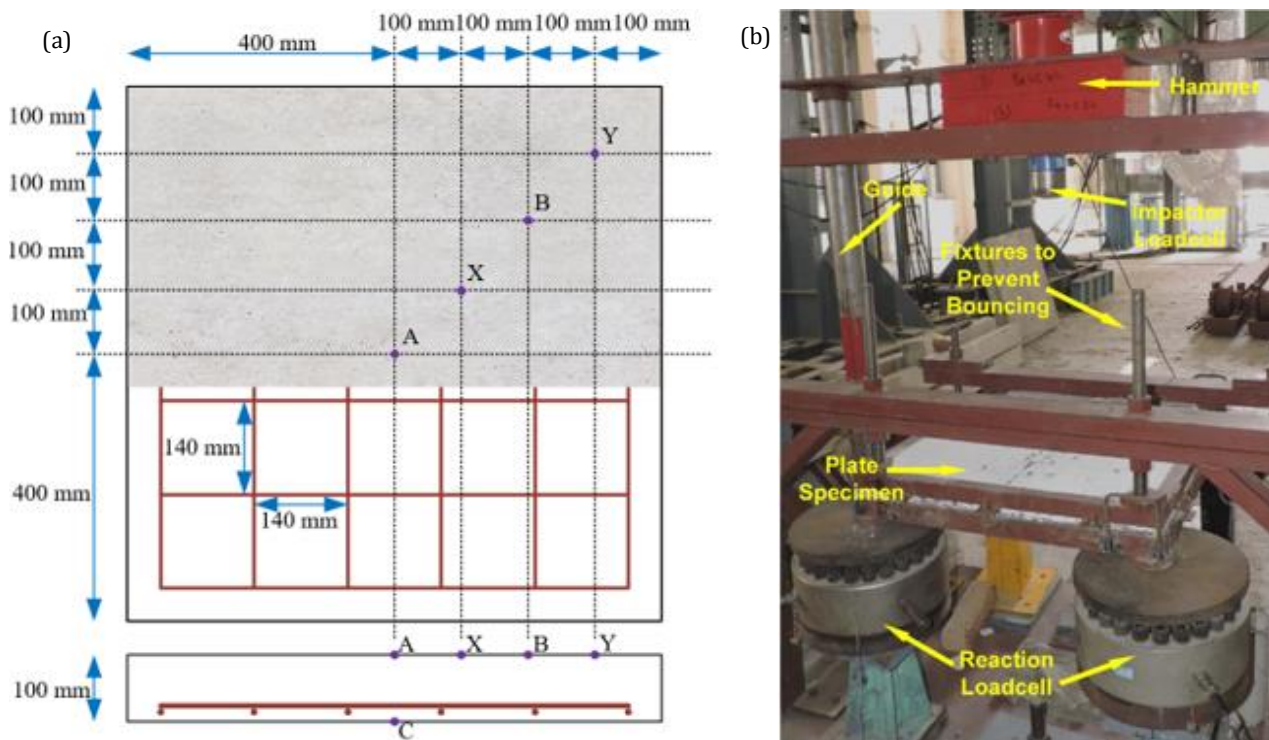
Fig. 2. (a) The geometric dimensions and rebar details of the RC slabs; (b) Test setup.

In the scope of the present FEM, it has been assumed the contact behavior between concrete and steel reinforcements was perfectly bonded using the keyword named *CONSTRAINED_LAGRANGE_IN_SOLID. It is determined from the mesh convergence study that when concrete element size is assumed as 20 mm, the results of numerical analysis convergence to those obtained by experiments. Besides, the mesh study indicates that further refinement has no considerable effect on the results although it causes more computational time. During the collision, firstly, the curved surface of the rigid hammer contacts the concrete. Thus, to represent actual behavior and calculate impact forces compatible with that of experiments, mesh refinement is required for the hammer. Mesh size has been assumed as 10 mm for the rigid ham-

mer. It should be emphasized here that the mesh size values which are chosen for the RC slab and the rigid hammer in the present FEM have been commonly used in previous studies for the RC slabs and the hammers, which are similar sizes (Şengel et al. 2022; Li et al. 2019, 2020).

The impact load was applied to the RC Slabs by defining the initial impact velocity to the hammer utilizing *INITIAL_VELOCITY_GENERATION keyword. In the experiments used for verification, impact velocities are given as 3.130 m/s and 4.427 m/s for drop heights of 500 mm and 1000 mm, respectively. These values have been assigned to the rigid hammer to apply impact forces to the RC slabs. Fig. 3 illustrates the FEM of the RC slab, steel reinforcement, rigid support, and rigid hammer.
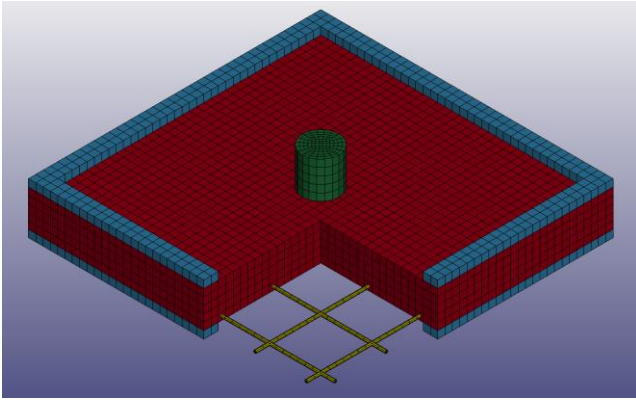
Fig. 3. The FEM of the rigid hammer, steel reinforcement, the RC slab, and the rigid support.

In the present FEM, concrete was modeled with the Winfrith material model (MAT_084-085). Winfrith concrete model was introduced for the nuclear industry to perform finite element analysis for the evaluation of the local and global response of the RC structures subjected to impact and blast loading and then implemented in LS-DYNA. This plasticity model is based on the shear failure surface presented by Ottosen (1977):

$$Y(I_1, J_2, J_3) = aJ_2 + \xi\sqrt{J_2} + bI_1 - 1 \qquad (1)$$

$$\xi = \begin{cases} k_1 \cos\left[\frac{1}{3}\cos^{-1}(k_2\cos(3\theta))\right] & \cos(3\theta) \geq 0 \\ k_1 \cos\left[\frac{\pi}{3} - \frac{1}{3}\cos^{-1}(-k_2\cos(3\theta))\right] & \cos(3\theta) \leq 0 \end{cases} \qquad (2)$$

where I_1 is the first invariant of stress tensor representing volumetric response, J_2 and J_3 are the second and third invariants of the deviatoric stress tensor. a, b, k_1 and k_2 are the functions of $T=f_t/f_c$ and these parameters can be determined from uniaxial, biaxial, and triaxial compression and uniaxial tension tests. f_t and f_c refer to tensile and compressive strengths of concrete, respectively. The meridional shape parameters a and b can be expressed using T and three non-dimensional constants, which are α=1.16, β=0.5907445, and γ=-0.613724, as follows (Maazoun et al. 2022):

$$b = \frac{1 + T\alpha\frac{\gamma}{3} - \alpha^2\frac{\gamma}{3} - \frac{\alpha}{T}}{\alpha^2\frac{\beta}{3} - 3\alpha - T\alpha\frac{\beta}{3}} \qquad (3)$$

$$a = \beta b + \gamma \qquad (4)$$

The k_1 and k_2 that defines the shape of the shear failure surface can be calculated as follows (Maazoun et al. 2022):

$$k_2 = \cos\left[3\tan^{-1}\left(\frac{1}{\sqrt{3}} - \frac{2h}{e\sqrt{3}}\right)\right] \qquad (5)$$

$$k_1 = \frac{e}{\cos\left[\frac{1}{3}\cos^{-1}(k_2)\right]} \qquad (6)$$

The e and h constants that take place in Eqs. (5) and (6) can be expressed as follows:

$$e = \frac{\sqrt{3}}{T}\left(1 - bT - T^2\frac{a}{3}\right) \qquad (7)$$

$$h = \frac{3 + 3b - a}{\sqrt{3}} \qquad (8)$$

Fig. 4(a) depicts the bi-linear concrete material model representing the uniaxial stress-strain relationship. The compression behavior of concrete was represented via the elastoplastic curve that has ultimate strain (ε_{cu}). While tension behavior was characterized as linear up to the peak tensile stress corresponding to cracking strain (ε_{cr}), the post-peak response was defined as a linear decrease. The ultimate tensile strain (ε_{tu}) was calculated based on the function of the concrete fracture energy (Thai and Kim 2014). The Winfrith model is capable of representing cracking, crushing, and shear retention behavior considering crack width and aggregate size and it is applied with eight-node continuum elements with a single integration point. The Winfrith model can capture crack generation, and the determination of crack is based on the theory presented by Wittman et al. (1988). When concrete tensile strength is exceeded, the crack occurs and propagates by generating a gap whose size is defined by crack width. The linear strain softening response can be characterized as in Fig. 4(b) with fracture energy (G_f), tensile strength (f_t), and crack width (w) (Maazoun et al. 2022).
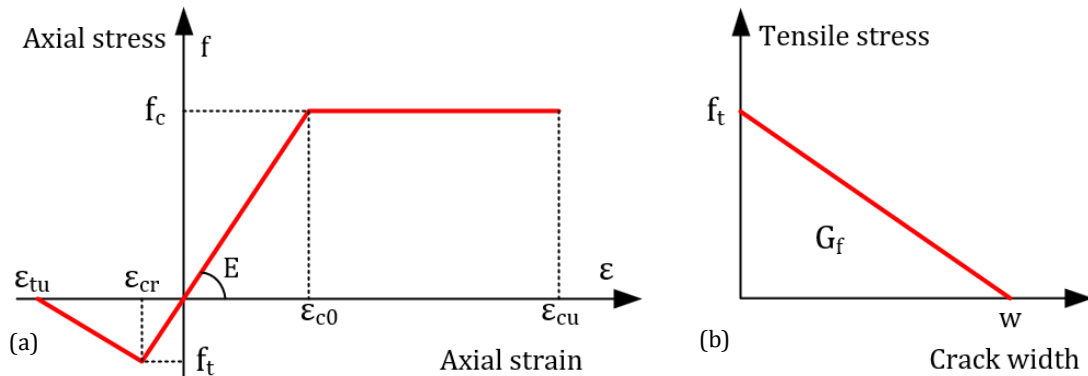
Fig. 4. (a) Stress-strain behavior of concrete; (b) Strain softening response.

The mass density (R0) 2400 kg/m³, tangent modulus (TM) 34000 MPa, Poisson's ratio (PR) 0.20, uniaxial compressive strength (UCS) 48.4 MPa, uniaxial tensile strength (UTS) and aggregate size (ASIZE) 10 mm are required input parameters for definition Winfrith concrete model, and the rest of parameters are calculated by LS-DYNA based on these values. In the numerical analysis, the tensile strength of concrete has been neglected, however, a small value is assigned to the tensile strength for the establishment of the material model. The steel reinforcements are defined with the elastic-plastic material model. The material card ∗MAT_PIECEWISE_LINEAR_PLASTICITY (MAT_24) allows users to define an arbitrary stress-strain curve for the representation of nonlinear behavior. The yield strength and elastic modulus belonging to steel material have been defined as 609 MPa and 200000 MPa, respectively. Poisson's ratio and density were 0.3 and 7850 kg/m³, respectively.

Impulsive loading such as impact and blast exhibits different behavior than static loading and it leads to an increase in the compressive and tensile strength of materials. The increase of material strength under high rate loading is known as the strain-rate effect (Hao et al. 2013; Sha and Hao 2013; Hao and Hao 2014; Malvar and Crawford 1998; Do et al. 2018a; CEB Code 1990). There exist many studies focused on the effect of the strain rate on the material properties, and accordingly the results of the finite element simulations in the literature. These studies unveil that the strain-rate effect should be regarded in the material model for the correct prediction of the dynamic responses and failure characteristics of structural elements exposed the impulsive loads (Li and Hao 2013; Li and Hao 2014; Chen et al. 2015; Jiang and Chorzepa 2015; Do et al. 2018a, 2018b). The strain rate effect is considered by multiplying the tensile and compression strengths belonging to steel and concrete material with a dynamic increase factor (DIF). The DIF refers to a ratio of dynamic strength to static strength and is defined for a wide spectrum of strain-rate values. A considerable number of empirical formulations have been developed to characterize the strain rate effect for concrete and steel materials in the literature (CEB 1990; Malvar 1998; Malvar and Ross 1998; Malvar and Crawford 1998; Fan et al. 2011; Hao and Hao 2014). The strain-rate effect can be included in the Winfrith concrete model via the option existing in its material card. For considered strain rate, the tensile (DIF_t) and compression (DIF_c) DIFs belonging to concrete, taking place in the Winfrith model, have been given in Eqs. (9) and (10) (Thai and Kim 2014).

$$DIF_t = \left(\frac{\dot{\varepsilon}}{\dot{\varepsilon}_{0T}}\right)^{1.016\delta} \text{ and } DIF_c = \left(\frac{\dot{\varepsilon}}{\dot{\varepsilon}_{0C}}\right)^{1.026\alpha}$$
$$\text{for } \dot{\varepsilon} < 30 \text{ s}^{-1} \quad (9)$$

$$DIF_t = \eta\dot{\varepsilon}^{1/3} \text{ and } DIF_c = \gamma\dot{\varepsilon}^{1/3} \text{ for } \dot{\varepsilon} > 30 \text{ s}^{-1} \quad (10)$$

The terms taking place in Eqs. (9) and (10) can be defined as follows:

$$\delta = \frac{1}{10+0.5f_C} \quad (11)$$

$$\alpha = \frac{1}{5+0.75f_C} \quad (12)$$

$$\log_{10}\eta = 6.933\delta - 0.492 \quad (13)$$

$$\log_{10}\gamma = 6.156\alpha - 0.49 \quad (14)$$

$$\dot{\varepsilon}_{0T} = 30x10^{-6} \text{ s}^{-1} \quad (15)$$

$$\dot{\varepsilon}_{0C} = 3x10^{-6} \text{ s}^{-1} \quad (16)$$

where f_c is the concrete cube strength and should be defined in a unit of MPa. Furthermore, the enhancement of elastic modulus with the effect of strain rate has (DIF_E) been considered in the Winfrith material model as follows:

$$DIF_E = 0.5\left[\left(\frac{\dot{\varepsilon}}{\dot{\varepsilon}_{0T}}\right)^{0.016} + \left(\frac{\dot{\varepsilon}}{\dot{\varepsilon}_{0C}}\right)^{0.026}\right] \quad (17)$$

Besides, ∗MAT_PIECEWISE_LINEAR_PLASTICITY (MAT_24) allows users to define the strain rate effect. The tensile and compression DIF relations of steel material have been defined according to equations proposed by Malvar (1998). For considered strain rate $\dot{\varepsilon}$, both tensile and compressive DIFs of steel material (DIF_{St}) can be calculated with Eq. (18).

$$DIF_{St} = \left(\frac{\dot{\varepsilon}}{10^{-4}}\right)^\mu \quad (18)$$

The μ coefficient existing in Eq. (18) can be written as based on the steel yield strength (f_y) as follows:

$$\mu = 0.074 - \frac{0.04f_y}{414} \quad (19)$$

In the FEM presented, the rigid material behavior has been assigned to the steel hammer and steel support. Also, all translational and rotational movements of rigid support were restrained. The RC slab was located between steel supports for clamping similar to that of experiments. The penalty-based ∗AUTOMATIC_SURFACE_TO_SURFACE contact algorithm was used for modeling the both contact between the rigid support and the RC slab and the contact between the rigid hammer and the RC slab. While for the contact between the rigid hammer and the RC slab, the contact stiffness scale factors were taken as 0.15, the contact stiffness scale factors were defined as 1.0 for the contact between the rigid support and the RC slab. Besides, the ∗AUTOMATIC_NODES_TO_SURFACE contact algorithm was used for modeling contact between hammer and steel reinforcements. A full bond between concrete and rebars was generated with ∗CONSTRAINED_LAGRANGE_IN_SOLID algorithm.

4. Parametric Study

In the scope of the parametric study, the FEM of the eight RC slabs with fixed support has been generated to investigate the effects of input impact energy, the location of the point at which impact load is applied, and the hammer geometry on the dynamic responses and failure characteristics of the RC slabs. Table 1 shows RC slab specimens used for the parametric study and the investigated parameters in the parametric study.

Table 1. RC slab test specimens and the investigated parameters

RC slabs	Drop height	Impact load application point	Hammer geometry
S1	500 mm	Center	Cylinder
S2	500 mm	Center	Hemisphere
S3	500 mm	Diagonal	Cylinder
S4	500 mm	Diagonal	Hemisphere
S5	1000 mm	Center	Cylinder
S6	1000 mm	Center	Hemisphere
S7	1000 mm	Diagonal	Cylinder
S8	1000 mm	Diagonal	Hemisphere

S1 and S5 test specimens are FEM of two RC slabs that have been tested in the experimental study conducted by Kumar et al. (2018), and they are used for verification of the present FEM. The geometric dimensions and reinforcement details were identical for these slabs and they had been presented in Fig. 2(a). The rest of the test specimens in the parametric study have also the same geometric dimensions and reinforcement details. Similar to the experimental program conducted by Kumar et al. (2018), input impact energies of 1.190 kJ and 2.380 kJ have been applied to the center of S1 and S5 (Point A in Fig. 2(a)), respectively, by assigning impact velocities of 3.130 m/s and 4.427 m/s to steel hammer with the weight of 242.85 kg. These two input impact energies have been assumed as one of the variables of the parametric study. However, the weight of the steel hammer has been kept constant for all RC slabs in numerical analysis. The second variable of the parametric study is the application point of the impact load. Two different impact load application points exist in numerical analysis. One is the center of the RC slabs (Point A in Fig. 2(a)) and another is the point at one-four of the diagonal line of the RC slabs (Point B in Fig. 2(b)). The last variable investigated in the parametric study is the geometric shape of the steel hammer. A cylinder hammer with a diameter of 100 mm which is taken place experimental program performed by Kumar et al. (2018) and a hemispheric hammer with a radius of 50 mm are two different hammer geometries that are included in the present FEM to investigate the effect of impactor geometry. It should be noted here that these two hammer geometries have the same weight of 242.85 kg. In the parametric analysis, under the effect of the applied input impact energy to the RC slabs, time-histories of the impact loads that act on RC slabs, and the displacements measured at the center of the RC slab were calculated. Besides, von-Misses stress distributions and crack patterns which have been obtained by the numerical analysis were presented. According to applied input impact energy, the impact forces, displacements, and load-displacement curves have been presented in Fig. 5. Besides, Table 2 summarizes the dynamic responses including peak impact forces, maximum and residual displacements, and the energy absorption capacities calculated from the area under the impact load versus displacement curves. Furthermore, Table 3 shows the comparison of the numerical results of S1 and S5 RC slabs and the experimental results presented in the study of Kumar et al. (2018).

Table 2. Dynamic responses obtained from numerical analysis

RC slabs	Peak impact forces (kN)	Max displacements (mm)	Residual displacements (mm)	Energy absorption capacities (J)
S1	273.26	10.58	5.51	1292.67
S2	99.41	12.74	8.64	1062.51
S3	264.03	2.50	0.70	398.56
S4	97.57	0.89	-0.23	76.06
S5	361.77	18.99	14.00	2640.56
S6	123.10	25.74	19.34	2195.39
S7	355.88	3.48	1.66	657.73
S8	119.93	0.93	-0.21	89.27
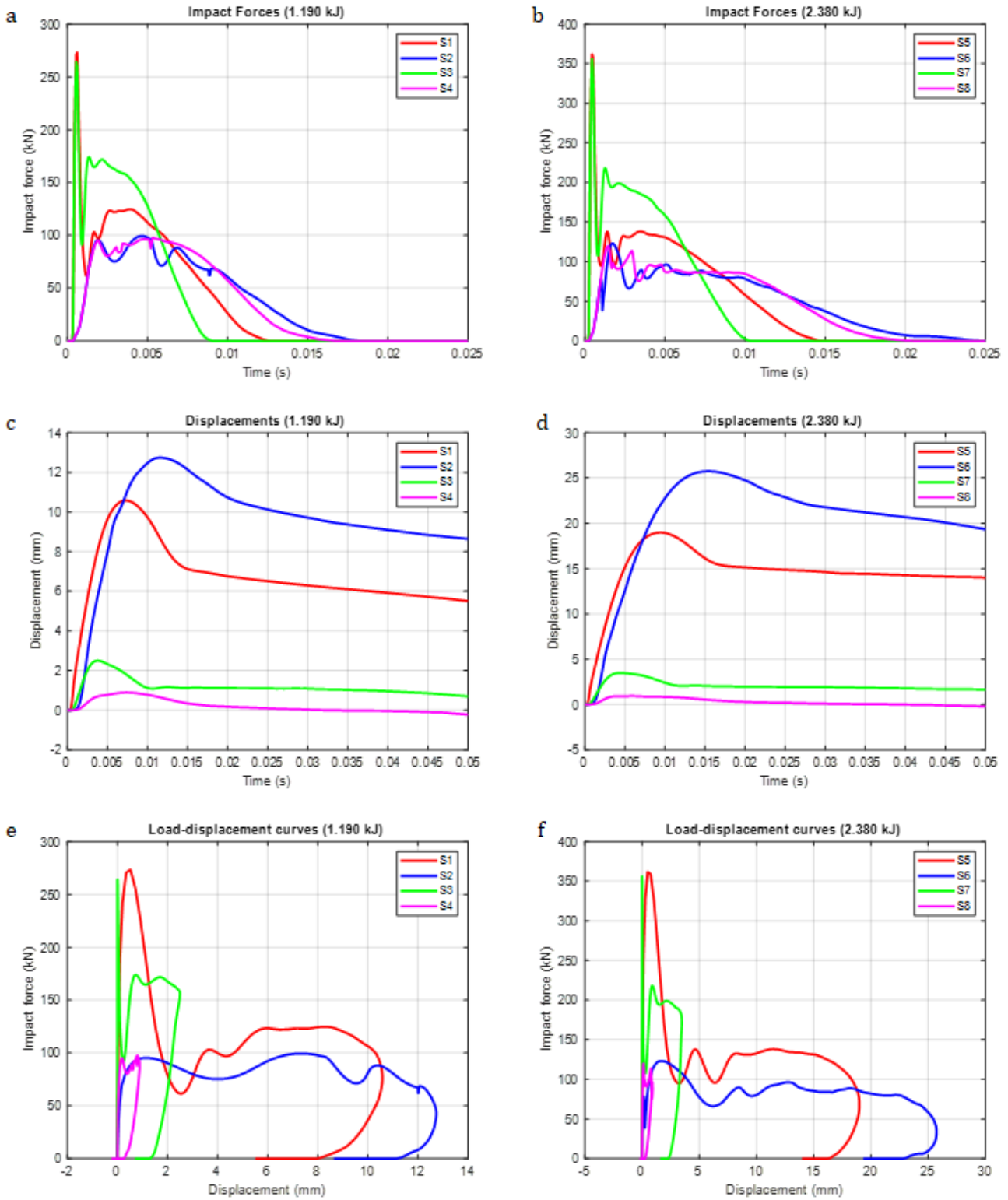
Fig. 5. (a) - (b) Time histories of impact forces; (c) - (d) Time histories of displacements; (e) - (f) Load-displacement curves.

Table 3. Comparison of numerical results and experimental results (Kumar et al. 2018).

RC slabs	Peak impact forces (kN)			Maximum mid-span displacements (mm)			Residual Displacements (mm)		
	Num.	Exp.	Ratio	Num.	Exp.	Ratio	Num.	Exp.	Ratio
S1	273.26	259.10	5%	10.58	9.76	8%	5.51	3.31	66%
S5	361.77	355.46	2%	18.99	19.97	5%	14.00	12.14	15%

When the results in Table 3 are examined, it is found that there is pretty good accordance between numerical and experimental results in terms of impact forces and maximum mid-span displacements. However, for residual displacements, there are up to 66% differences between numerical and experimental results. It should be also emphasized that when applied input impact energy is increased, this difference has become remarkably lower. Authors consider that alongside the good accordance between numerical and experimental results, which were observed for impact forces and maximum displacements, the differences in residual displacements are also acceptable for impact simulations where loading occurs in a very short time. Many factors such as the non-homogeneous nature of concrete, rigors on accurate estimation of strain-rate effect and damping of materials, and exact support conditions in numerical analysis contrary to real support conditions that have included many frictional movements, the complex interaction between contact areas during the collision may lead to differences numerical and experimental results. Furthermore, similar acceptable differences between numerical and experimental residual displacements have been observed in the comprehensive numerical studies in the literature (Othman and Marzouk 2014; Huang et al. 2021; Liu et al. 2020; Batarlar and Saatci 2022). Eventually, it is thought that the presented FEM could be safely used for impact responses of the RC slabs with fixed support.

When the numerical results are examined, it is found that for both applied input impact energy the application point of impact load has a quite negligible effect on the maximum impact forces. When impact load is applied to Point B instead of Point A, the decrease in maximum impact load is under 3.3%. However, the application of impact load on Point B instead of A decreased the mid-span maximum and residual displacements, and energy absorption capacities considerably, especially when high impact energy is applied. For high input impact energy, shifting impact load to Point B, decreased the mid-span maximum and residual displacements, and energy absorption capacities 28 times, 92 times, and 25 times, respectively. Eccentric impact loading has led to less maximum and residual displacement on account of the restraint provided by the supporting (Anas et al. 2022c).

Numerical results show that the cylinder hammer produces the greater maximum impact forces, however, impact duration is shorter. A similar tendency has been reported in the previous comprehensive analytical study (Li et al. 2019). When results are examined, it is determined that the cylinder hammer led to approximately 2.7-3.0 times greater impact forces. However, mid-span maximum and residual displacement increased with the use of the hemispheric hammer. As a result of impact load and displacement tendencies, the energy absorption of the RC slabs subjected impact load applied using a cylinder hammer is greater and they experience more ductile behavior. Furthermore, there is an important issue related to maximum and residual displacements that should be explained. As above mentioned, the impact load applied with a hemispheric hammer cause higher displacement values, however, this is true when the displacement measurement has been taken from near the

collision region which is the surrounding area of the impact load application point (Li et al. 2019). Otherwise, this behavior tendency becomes reverse and the cylinder hammer generates higher displacements. For example, when the impact load is applied to point B, if the maximum and residual displacements at mid-span, which is relatively far from impact point B, are examined, it is seen that S3 and S7 exhibit greater displacement than S4 and S8, respectively. For a better understanding of this behavior tendency, the maximum displacement measurements taken from four points on the diagonal of the S5 and S6 test specimens have been presented in Fig. 6. Impact loads had been applied to the slab center of these specimens. When Fig. 6 is examined, it is found while in the collision zone, the hemisphere hammer generates higher displacement values, but away from this region cylinder hammer causes maximum displacements. Hemisphere hammer leads to localize damage with its penetrative effect and correspondingly increased the displacements that occurred in the collision zone. Away from the collision zone, the local damage effect of the hemisphere hammer remarkable decrease, cylinder hammer which produces greater impact forces becomes more effective on displacements.
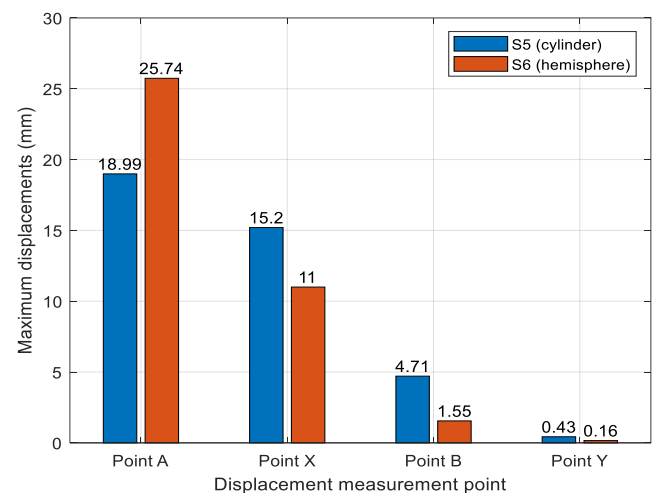
Fig. 6. The comparison of the maximum displacements measured at the diagonal of the S5 and S6.

When impact energy applied to the RC slabs is increased, the force transferred to the slabs and damages occurred also increased, and thus, the maximum and residual displacements, and energy absorption capacities increased. With the increase of input impact energy, while maximum impact forces increase up to 35%, maximum and residual displacements increased up to 2 and 2.5 times, respectively. Besides, it is found that the energy absorption capacities increased 1.2-2.1 times with the effect of higher input impact energy applied. Fig. 7 illustrates von-Misses stress distributions and crack patterns obtained from numerical analysis. It is seen from Fig. 7 that damage is concentrated more collision region. Besides, while cylinder hammers cause more damage, the hemisphere hammer leads to penetrative local damaged. The increase of impact energy applied to slabs remarkably increased the damages.
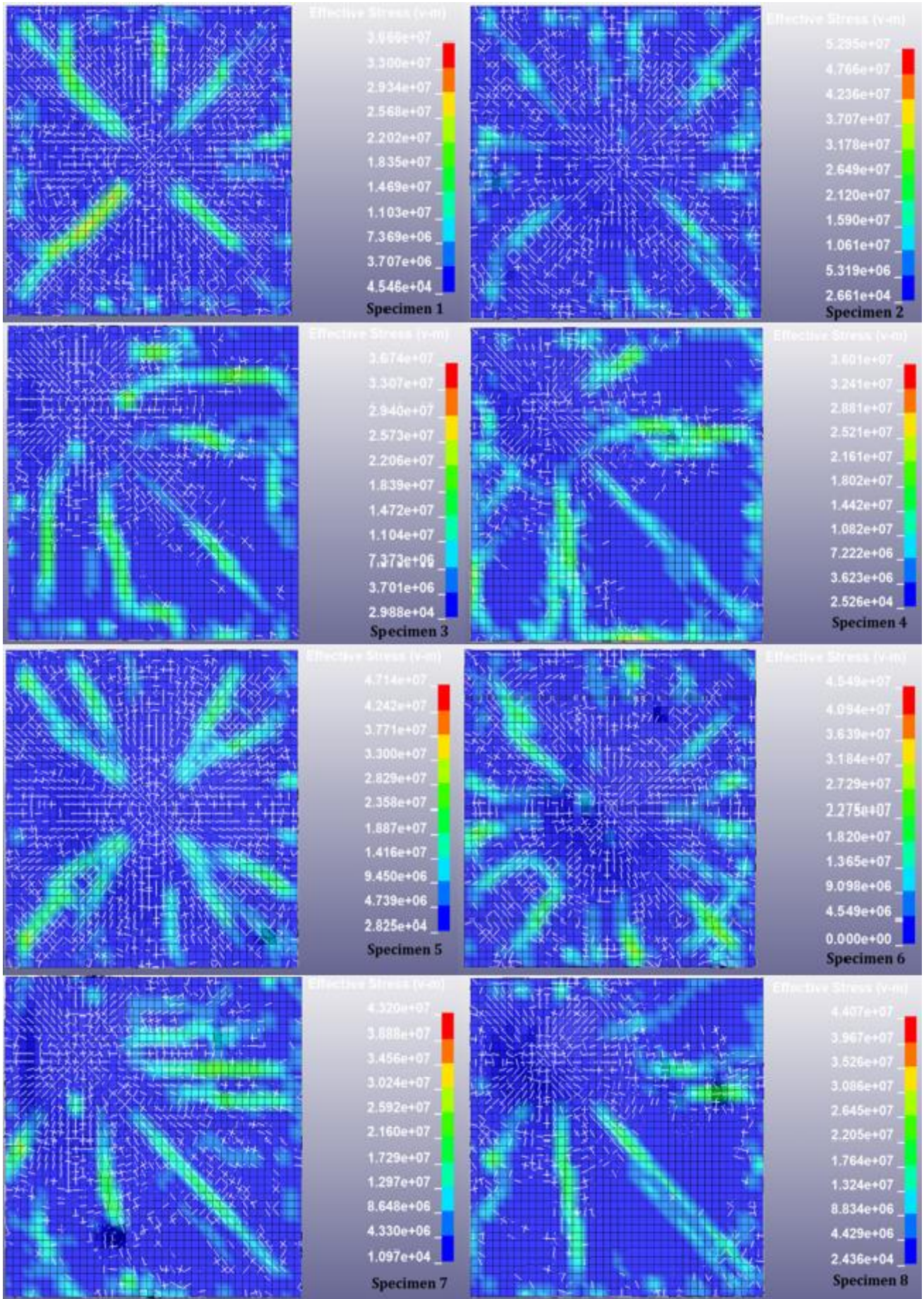
Fig. 7. von-Misses stress distributions and crack patterns obtained numerical analysis.

5. Conclusion

The present study introduces a detailed FEM including strain-rate effect, and crack visualization algorithm for evaluation of the RC slabs with fixed support under the effect of impact load. The proposed FEM has been verified with experimental results existing in a study previously presented in the literature. Then, a parametric study where the effects of impact energy applied, the impact load application point, and the hammer geometry on the dynamic responses and failure characteristics of the RC slabs are investigated. The results obtained from the parametric analysis are summarized below:

- The application point of impact load has a quite negligible effect on the maximum impact forces. However, instead of slab center, eccentric impact loading generates less mid-span maximum and residual displacements and energy absorption capacities.
- Impact loading with a cylinder hammer causes greater impact forces however impact duration becomes short. The cylinder hammer led to approximately 2.7-3.0 times greater impact forces. When the displacement measurement has been taken from the near field of the impact load application point, the hemispheric hammer causes higher displacement values due to localize damage thanks to its penetrative behavior. However, for the displacement measurements away from the collision zone, it is observed that the cylinder hammer yields higher displacement responses.
- With the increase of impact energy applied, the maximum impact forces increase up to 35%, while maximum and residual displacements, and the energy absorption capacities up to 2, 2.5, and 2.1 times, respectively.
- The authors also consider that for the future studies present FEM could be improved with the implementation of the bond-slip model instead of the assumption of the perfect bond between the concrete and reinforcement.

Acknowledgements

Funding

Conflict of Interest

The authors declared no potential conflicts of interest with respect to the research, authorship, and/or publication of this manuscript.

REFERENCES

Al Rawi Y, Temsah Y, Baalbaki O, Jahami A, Darwiche M (2020). Experimental investigation on the effect of impact loading on behavior of post- tensioned concrete slabs. *Journal of Building Engineering,* 31, 101207.

Almusallam T, Al-Salloum Y, Alsayed S, Iqbal R, Abbas H (2015). Effect of CFRP strengthening on the response of RC slabs to hard projectile impact. *Nuclear Engineering and Design*, 286, 211–226.

Anas SM, Alam M, Umair M (2022a). Effect of design strength parameters of conventional two-way singly reinforced concrete slab under concentric impact loading. *Materials Today: Proceedings,* 62, 2038–2045.

Anas SM, Alam M, Tahzeeb R (2022b). Impact response prediction of square RC slab of normal strength concrete strengthened with (1) laminates of (i) mild-steel and (ii) C-FRP, and (2) strips of C-FRP under falling-weight load. *Materials Today: Proceedings,* In Press.

Anas SM, Alam M, Shariq M (2022c). Damage response of conventionally reinforced two-way spanning concrete slab under eccentric impacting drop weight loading. *Defence Technology,* In Press.

Anil Ö, Kantar E, Yilmaz MC (2015). Low velocity impact behavior of RC slabs with different support types. *Construction and Building Materials*, 93, 1078–1088.

Batarlar B, Saatci S (2022). Numerical investigation on the behavior of reinforced concrete slabs strengthened with carbon fiber textile reinforcement under impact loads. *Structures*, 41, 1164–1177.

CEB-FIP Model Code 90 (1993). Comite Euro-International du Beton, Thomas Telford Ltd., London.

Chen W, Hao H, Chen S (2015). Numerical analysis of prestressed reinforced concrete beam subjected to blast loading. *Materials and Design*, 65, 662–674.

Chen W, Pham TM, Elchalakani M, Li H, Hao H, Chen L (2020). Experimental and numerical study of basalt FRP strip strengthened RC slabs under impact loads. *International Journal of Structural Stability and Dynamics*, 2040001.

Daneshvar K, Moradi MJ, Ahmadi K, Hajiloo H (2021). Strengthening of corroded reinforced concrete slabs under multi-impact loading: Experimental results and numerical analysis. *Construction and Building Materials*, 284, 122650.

Do TV, Pham TM, Hao H (2018a). Dynamic responses and failure modes of bridge columns under vehicle collision. *Engineering Structures*, 156, 243–259.

Do TV, Pham TM, Hao H (2018b). Numerical investigation of the behavior of precast concrete segmental columns subjected to vehicle collision. *Engineering Structures*, 156, 375–393.

Fan W, Yuan W, Yang Z, Fan Q (2011). Dynamic demand of bridge structure subjected to vessel impact using simplified interaction model. *Journal of Bridge Engineering*, 16(1), 117–126.

Hao Y, Hao H (2014). Influence of the concrete DIF model on the numerical predictions of RC wall responses to blast loadings. *Engineering Structures*, 73, 24–38.

Hao Y, Hao H, Jiang GP, Zhou Y (2013). Experimental confirmation of some factors influencing dynamic concrete compressive strengths in high-speed impact tests. *Cement and Concrete Research*, 52, 63–70.

Hering M, Bracklow F, Kühn T, Curbach M (2020). Impact experiments with reinforced concrete plates of different thicknesses. *Structural Concrete*, 21(2), 587–598.

Huang Z, Chen W, Tran TT, Pham TM, Hao H, Chen Z, Elchalakani M (2021). Experimental and numerical study on concrete beams reinforced with Basalt FRP bars under static and impact loads. *Composite Structures*, 263, 113648.

Jiang H, Chorzepa MG (2015). An effective numerical simulation methodology to predict the impact response of pre-stressed concrete members. *Engineering Failure Analysis*, 55, 63–78.

Kumar V, Iqbal MA, Mittal AK (2018). Experimental investigation of prestressed and reinforced concrete plates under falling weight impactor. *Thin-Walled Structures*, 126, 106–116.

Li H, Chen W, Hao H (2019). Influence of drop weight geometry and interlayer on impact behavior of RC beams. *International Journal of Impact Engineering*, 131, 222–237.

Li H, Chen W, Hao H (2020). Factors influencing impact force profile and measurement accuracy in drop weight impact tests. *International Journal of Impact Engineering*, 145, 103688.

Li H, Chen W, Pham TM, Hao H (2021). Analytical and numerical studies on impact force profile of RC beam under drop weight impact. *International Journal of Impact Engineering*, 147, 103743.

Li J, Hao H (2013). Influence of brittle shear damage on accuracy of the two-step method in prediction of structural response to blast loads. *International Journal of Impact Engineering*, 54, 217–231.

Li J, Hao H (2014). Numerical study of concrete spall damage to blast loads. *International Journal of Impact Engineering*, 68, 41–55.

Li J, Hao H, Wu C (2017). Numerical study of precast segmental column under blast loads. *Engineering Structures*, 134, 125–137.

Liu B, Fan W, Huang X, Shao X, Kang L (2020). A simplified method to predict damage of axially-loaded circular RC columns under lateral impact loading. *International Journal of Concrete Structures and Materials*, 14(32), 1–24.

Maazoun A, Matthys S, Atoui O, Belkassem B, Lecompte D (2022). Finite element modelling of RC slabs retrofitted with CFRP strips under blast loading. *Engineering Structures*, 252, 113597.

Malvar LJ, Ross CA (1998). Review of strain rate effects for concrete in tension. *ACI Materials Journal*, 95(6), 735–739.

Malvar LJ (1998). Review of static and dynamic properties of steel reinforcing bars. *ACI Materials Journal,* 95(5), 609–616.

Malvar LJ, Crawford JE (1998). Dynamic increase factors for concrete. *DTIC Document*, 1998.

Marzouk HOH (2014). Numerical investigation of reinforced concrete slabs under impact loading. *Proceedings of the 10th Fib International PhD Symposium in Civil Engineering*, Canada.

Mizushima Y, Iino N (2022). Behavior of thin reinforced concrete slabs and effect of reinforcement bars subjected low-velocity impact. *Structures*, 38, 832–847.

Mousavi T, Shafei E (2019). Impact response of hybrid FRP-steel reinforced concrete slabs. *Structures*, 19, 436–448.

Ottosen NS (1977). A Failure Criterion for Concrete. *ASCE Journal of the Engineering Mechanics Division*, 103(4), 527–535.

Radnić J, Matešan D, Grgić N, Baloević G (2015). Impact testing of RC slabs strengthened with CFRP strips. *Composite Structures*, 121, 90–103.

Sadraie H, Khaloo A, Soltani H (2019). Dynamic performance of concrete slabs reinforced with steel and GFRP bars under impact loading. *Engineering Structures*, 191, 62–81.

Said AMI, Mouwainea EM (2022). Experimental investigation on reinforced concrete slabs under high-mass low velocity repeated impact loads. *Structures*, 35, 314–324.

Şengel S, Erol H, Yılmaz T, Anıl Ö (2022). Investigation of the effects of impactor geometry on impact behavior of reinforced concrete slabs. *Engineering Structures*, 263, 114429.

Sha Y, Hao H (2013). Laboratory tests and numerical simulations of barge impact on circular reinforced concrete piers. *Engineering Structures*, 46, 593–605.

Shi C, Zhang J, Zhang J, Shao F, Zhang Y, Zhang M (2021). Experimental study and numerical analysis on impact resistance of civil air defense engineering shear wall. *Advances in Civil Engineering*, 2021, 7376909.

Soltani H, Khaloo A, Sadraie H (2020). Dynamic performance enhancement of RC slabs by steel fibers vs. externally bonded GFRP sheets under impact loading. *Engineering Structures*, 213, 110539.

Thai DK, Kim SE (2014). Failure analysis of reinforced concrete walls under impact loading using the finite element approach. *Engineering Failure Analysis*, 45, 252–277.

Thai DK, Kim SE (2017). Numerical simulation of pre-stressed concrete slab subjected to moderate velocity impact loading. *Engineering Failure Analysis*, 79, 820–835.

Vijay TJ, Kumar MM, Sofia G, Abiraami R (2020). Impact behaviour of reinforced concrete slabs embedded with inclined reinforcements. *Materials Today: Proceedings,* In Press.

Wittmann FH, Rokugo K, Brühwiler E, Mihashi H, Simonin P (1988). Fracture energy and strain softening of concrete as determined by means of compact tension specimens. *Materials and Structures*, 21(1), 21–32.

Yilmaz T, Anıl Ö, Erdem RT (2022). Experimental and numerical investigation of impact behavior of RC slab with different opening size and layout. *Structures*, 35, 818–832.

Yilmaz T, Kiraç N, Anil Ö (2019). Experimental investigation of axially loaded reinforced concrete square column subjected to lateral low-velocity impact loading. *Structural Concrete*, 20(4), 1358–1378.

Yılmaz T, Kirac N, Anil Ö, Erdem RT, Kacaran G (2020). Experimental investigation of impact behaviour of RC Slab with different reinforcement ratios. *KSCE Journal of Civil Engineering*, 24(1), 241–254.

Yılmaz T, Kıraç N, Anil Ö, Erdem RT, Sezer C (2018). Low-velocity impact behaviour of two way RC slab strengthening with CFRP strips. *Construction and Building Materials*, 186, 1046–1063.

Yılmaz T, Kıraç N, Anıl Ö, Erdem RT, Hoşkal V (2020). Experimental and numerical investigation of impact behavior of reinforced concrete slab with different support conditions. *Structural Concrete*, 21(6), 2689–2707.